Giant star-forming clumps?

R. J. Ivison, J. Richard, A. D. Biggs, M. A. Zwaan, E. Falgarone, V. Arumugam, P. P. van der Werf, W. Rujopakarn

Monthly Notices
of the
ROYAL ASTRONOMICAL SOCIETY

MNRAS **495,** L1–L6 (2020)
Advance Access publication 2020 March 16

doi:10.1093/mnrasl/slaa046

Giant star-forming clumps?

R. J. Ivison [1]★ J. Richard,[2] A. D. Biggs [1] M. A. Zwaan,[1] E. Falgarone,[3] V. Arumugam,[1,4] P. P. van der Werf[5] and W. Rujopakarn[6,7]

[1]*European Southern Observatory, Karl-Schwarzschild-Strasse 2, D-85748 Garching, Germany*
[2]*Univ Lyon, Univ Lyon1, Ens de Lyon, CNRS, Centre de Recherche Astrophysique de Lyon UMR5574, F-69230 Saint-Genis-Laval, France*
[3]*Laboratoire de Physique de l'ENS, ENS, Université PSL, CNRS, Sorbonne Université, Université Paris-Diderot, Sorbonne Paris Cité, F-75005 Paris, France*
[4]*Institut de Radioastronomie Millimétrique, 300 rue de la Piscine, F-38406 Saint-Martin d'Hères, France*
[5]*Leiden Observatory, Leiden University, P.O. Box 9513, NL-2300 RA Leiden, the Netherlands*
[6]*Department of Physics, Faculty of Science, Chulalongkorn University, 254 Phayathai Road, Pathumwan, Bangkok TH-10330, Thailand*
[7]*National Astronomical Research Institute of Thailand (Public Organisation), Don Kaeo, Mae Rim, Chiang Mai TH-50180, Thailand*

Accepted 2020 March 12. Received 2020 March 12; in original form 2019 December 19

ABSTRACT

With the spatial resolution of the Atacama Large Millimetre Array (ALMA), dusty galaxies in the distant Universe typically appear as single, compact blobs of dust emission, with a median half-light radius, ≈1 kpc. Occasionally, strong gravitational lensing by foreground galaxies or galaxy clusters has probed spatial scales 1–2 orders of magnitude smaller, often revealing late-stage mergers, sometimes with tantalizing hints of sub-structure. One lensed galaxy in particular, the Cosmic Eyelash at $z = 2.3$, has been cited extensively as an example of where the interstellar medium exhibits obvious, pronounced clumps, on a spatial scale of ≈100 pc. Seven orders of magnitude more luminous than giant molecular clouds in the local Universe, these features are presented as circumstantial evidence that the blue clumps observed in many $z \sim 2$–3 galaxies are important sites of ongoing star formation, with significant masses of gas and stars. Here, we present data from ALMA which reveal that the dust continuum of the Cosmic Eyelash is in fact smooth and can be reproduced using two Sérsic profiles with effective radii, 1.2 and 4.4 kpc, with no evidence of significant star-forming clumps down to a spatial scale of ≈80 pc and a star formation rate of $<3\,M_\odot\,yr^{-1}$.

Key words: galaxies: high-redshift – galaxies: starburst – galaxies: structure – infrared: galaxies – submillimetre: galaxies.

1 INTRODUCTION

Interferometric submillimetre (submm) observations of distant, dusty star-forming galaxies (DSFGs, sometimes known as submm-selected galaxies – SMGs) – intense starbursts with star formation rates (SFRs) in excess of $100\,M_\odot\,yr^{-1}$ – have revealed a consistent morphological picture. Ignoring multiplicity and signatures associated with galaxy interactions and mergers, of which there are many examples, the thermal continuum emission from each is usually dominated by a single, compact blob of dust – expected to be largely co-spatial with the molecular gas – with a median half-light radius, 0.2–0.3 arcsec or ≈1 kpc (Ikarashi et al. 2015, 2017; Simpson et al. 2015; Hodge et al. 2016; Oteo et al. 2016, 2017a; Rujopakarn et al. 2016; Gullberg et al. 2018; Ma et al. 2019; Rujopakarn et al. 2019).

In a handful of cases, it has been possible to probe spatial scales nearly an order of magnitude smaller, ≈150 pc or ≈20 milliarcsec (mas), using the longest available baselines, aided in one case by a bright, compact, in-beam calibrator (Oteo et al. 2017b). The findings are consistent – compact blobs of dust emission, occasionally multiple blobs suggestive of mid-stage mergers (Iono et al. 2016; Tadaki et al. 2018). There have been glimpses of sub-structure, interpreted by some as potential evidence for spiral arms, bars, and rings caused by tidal disturbances (Hodge et al. 2019), though some simulations and alternative analyses suggest that we should be cautious of their reality, or that they may instead be evidence of mergers at a later stage (e.g. Rujopakarn et al. 2019).

Strong gravitational lensing by foreground galaxies or galaxy clusters allows us to probe spatial scales an order of magnitude smaller still, at least in theory. The first of the three most celebrated cases is that of H-ATLAS J090311.6+003906, or SDP.81, which lies at $z = 3.0$ and is amplified by a single foreground galaxy ($\mu \approx 15$, Dye et al. 2015; Rybak et al. 2015a, possibly with a $\sim 10^9$-$M_\odot$ dark-matter subhalo – Hezaveh et al. 2016). Dye et al. (2015) and Rybak et al. (2015b) found evidence of a galaxy interaction (as with most bright SMGs – Engel et al. 2010), in this case a late-stage merger between a rotating disc of dusty gas and a

★ E-mail: rob.ivison@eso.org

neighbouring galaxy seen only in the near-infrared (rest-frame optical). Intriguingly, there is evidence that the disc is fragmenting, since Swinbank et al. (2015) identify up to five submm-emitting dust clumps, several of which can be seen at multiple frequencies, on approximately the scale of the synthesized beam (≈150 mas, or ≈200 pc), which supports more ambiguous evidence[1] from maps of CO(5–4) and CO(8–7) that the gas distribution is clumpy.

Even more robust, though difficult to visualize because of the extreme gravitational amplification that gives rise to its name, are the dozen or more molecular clouds uncovered by recent 0.2-arcsec FWHM imaging in CO(4–3) of the Cosmic Snake, at $z = 1.036$, by Dessauges-Zavadsky et al. (2019). Each of these clouds is at least an order of magnitude more massive and turbulent than those in the Milky Way today, and there is a substantial spatial disconnect between the gas and the twenty clumps seen in *Hubble Space Telescope* imaging (Cava et al. 2018) which Dessauges-Zavadsky et al. had expected to detect in CO.

Cited extensively as the definitive example of where the interstellar medium (ISM) exhibits dusty star-forming clumps is the case of SMM J21352−0102, or the Cosmic Eyelash, named due to its shape and its proximity to the Cosmic Eye (Smail et al. 2007; Swinbank et al. 2010). The Cosmic Eyelash lies behind the $z = 0.325$ galaxy cluster, MACS J2135−01, which amplifies it gravitationally by a factor, $\mu = 37.5$. With its spectral energy distribution (SED) peaking at $\lambda_{\rm obs} \approx 350$ μm at a flux density, ≈500 mJy (Ivison et al. 2010) – so typical intrinsically of an SMG close to the confusion limit for a 10–15-m single dish – and with an SED that has proved invaluable for FIR/submm photometric redshift estimation (e.g. González-Nuevo et al. 2019), it was the first SMG sufficiently bright to allow a blind redshift to be obtained, $z = 2.3$. This was determined by Swinbank et al. (2010) via detection of CO $J = 1$–0 using the *Green Bank Telescope*, a few months ahead of the blind detection of CO $J = 3$–2 and $J = 5$–4 from SMM J14009+0252 by Weiß et al. (2009). The Cosmic Eyelash was also sufficiently bright to allow FIR spectroscopy with the *Herschel* SPIRE FTS (George et al. 2014; Zhang et al. 2018a). Early interferometric follow-up by Swinbank et al. (2010), using the eight-element Submillimeter Array in its most extended (VEX) configuration, provided evidence of at least five and as many as eight bright, compact, dusty clumps. The most tempting lensing configuration suggested four on each side of a caustic, each with an intrinsic spatial scale of ≈100 pc, where the morphology of the molecular gas seen in later imaging by Swinbank et al. (2011) was described as 'broadly aligned' with the continuum clumps.

More than any other submm data, the discovery of these dust clumps in the Cosmic Eyelash has been cited (even quite recently – Guo et al. 2018; Meng & Gnedin 2019) as circumstantial evidence that the giant (≈0.1–1 kpc) off-centre clumps – typically found in broad-band rest-frame ultraviolet (UV)–optical images of $z \approx 1$–3 galaxies (e.g. Cowie, Hu & Songaila 1995; Conselice et al. 2004; Elmegreen & Elmegreen 2005; Elmegreen, Bournaud & Elmegreen 2008; Genzel et al. 2011; Elmegreen et al. 2013), and especially in IR-luminous galaxies (Calabrò et al. 2019) – are important sites of star formation, albeit perhaps short-lived (Genel et al. 2012; Chevance et al. 2020, cf. Bournaud et al. 2014; Kruijssen et al. 2019). Bright in Hα (Livermore et al. 2012, 2015), these blue clumps are thought to harbour significant star formation[2] (though less than 10 per cent of the galaxy total – Guo et al. 2018) as well as significant quantities of stars ($M\star \approx 10^7$−10^9 M$\odot$ − Guo et al. 2012, 2015, 2018; Dessauges-Zavadsky et al. 2017; Cava et al. 2018; Dessauges-Zavadsky & Adamo 2018, cf. Wuyts et al. 2012; Zanella et al. 2019; Larson et al. 2020) and any residual molecular gas from which those stars formed. On the other hand, simulations in UV and Hα light (e.g. Tamburello et al. 2017; Meng & Gnedin 2019) and some data at longer wavelengths – less susceptible to the pernicious effects of dust – suggest that some of the best-known examples of star-forming clumps may have masses and sizes that have been overestimated and are likely rather insignificant, plausibly even the result of patchy dust obscuration, e.g. UDF11 in Rujopakarn et al. (2016) and UDF6462 in Cibinel et al. (2017).

In this paper, we present new observations obtained using the Atacama Large Millimetre/Submillimetre Array (ALMA) which reveal that around 99 per cent of the dust continuum emission from the Cosmic Eyelash is in fact distributed smoothly. This paper is organized as follows: Section 2 describes the observations and data-reduction, and Section 3 presents the fundamental result. In Section 4, we discuss our lens modelling of the observed images. We summarize and draw conclusions in Section 5. Throughout, we adopt the Chabrier (2003) initial mass function and a standard Λ cold dark matter cosmology with $\Omega_{\rm m} = 0.3$, $\Omega_\Lambda = 0.7$, and $H_0 = 70\,{\rm km\,s^{-1}\,Mpc^{-1}}$, where 1 arcsec at $z = 2.3$ corresponds to 8.2 kpc.

2 OBSERVATIONS AND DATA REDUCTION

The Cosmic Eyelash has been observed several times with ALMA, predominantly in bands 6 and 7. From these, we have selected a subset with good sensitivity (≤ 50 μJy beam^{-1}) and angular resolution ($\Delta\theta \leq 0.3$ arcsec). Although mostly designed to observe various molecular transitions, these data contain a significant fraction of line-free channels that allow sensitive continuum maps to be made. One project used ALMA's maximum-bandwidth ($\Delta\nu = 7.5$ GHz) 'single-continuum' (SC) mode and – although a little less sensitive than the others, due to less observing time – contains both an extended and compact configuration and is thus particularly sensitive to low-brightness extended emission. All observations were conducted in dual-polarization mode with low-spectral-resolution time-division mode spectral windows, i.e. with 2 GHz of usable bandwidth. See Table 1 for a summary of the band-6 and band-7 ALMA observations considered for our study.

Data reduction was carried out using the Common Astronomy Software Application package, with calibration performed using the ALMA Science Pipeline. Contamination from molecular lines was identified by combining all baselines to produce a spectrum, with affected channel ranges then flagged. Imaging was performed subsequently, using TCLEAN with a Briggs weighting scheme (ROBUST $= -0.5$). Self-calibration was used (first in phase, then in amplitude and phase) to produce the final continuum maps. Each configuration of the 2012.1.01029.S data was mapped and self-calibrated separately. Additional self-calibration of the combined datasets was necessary to correct for small errors in the relative astrometry and flux-density scales.

[1]Due to the possibility of excitation effects, or the patchy destruction of CO by cosmic rays (e.g. Bisbas et al. 2017).

[2]One might ask why, since with adequate spatial resolution we generally find a disconnect between active star formation and blue light, and would anyway expect the dusty gas to be expelled rapidly, post-starburst, such that the ratio of UV to submm clumps may reflect the lifetimes for each phase.

Table 1. ALMA observations of the Cosmic Eyelash in bands 6 and 7.

ALMA project	Detected species[a]	ν_0[b] (GHz)	σ (μJy beam^{-1})[c]	Beam[d] (mas^2)
2012.1.00175.S	OH^+, H_2O	303.9	27	174×148[e]
2012.1.00175.S	H_2O	356.4	48	232×167
2012.1.01029.S	SC	345.0	60	282×246
2016.1.00282.S	CH^+	251.0	21	225×160

[a]SC refers to a 'single-continuum' set up.
[b]Average frequency, after flagging of line-contaminated channels.
[c]Continuum sensitivity.
[d]Synthesized beam size, FWHM.
[e]For the average magnifications across the Cosmic Eyelash, this corresponds to linear scales along the major and minor axes of 130 and 820 pc in the source plane, respectively.

The most sensitive map was obtained from the band-6 data (rest-frame 360 μm, where we probe emission from cold dust), published previously as part of a survey of luminous, dusty galaxies in the CH^+ line (Falgarone et al. 2017). The r.m.s. noise level was $\sigma = 21$ μJy beam^{-1} and the synthesized beam measured 0.23×0.16 arcsec^2 (full width at half-maximum), with the major axis at a position angle (PA, measured East of North) of 93°.

In band 7, the map with the best sensitivity and highest angular resolution was that produced from the 2012.1.00175.S data, intended originally to trace OH^+ and H_2O (average frequency, 303.9 GHz; rest frame 300 μm). A continuum map of these data has already been published by Indriolo et al. (2018) but our map has a significantly higher dynamic range and a sensitivity of $\sigma = 27$ μJy beam^{-1}. The synthesized beam was somewhat smaller than that of the band-6 map, 0.17×0.15 arcsec^2 at PA = 66°. A second data set from the same project, targeting H_2O at a higher frequency, 356.4 GHz, produced a similar map, though not quite as sensitive. The synthesized beam of the band-7 pure-continuum map was competitive with the other maps, 0.28×0.25 arcsec^2, PA = 104°, with a sensitivity of $\sigma = 60$ μJy beam^{-1}.

3 RESULTS

We quickly and simply illustrate the purpose of this paper in Fig. 1, which shows the SMA image[3] of Swinbank et al. (2010) alongside our deep ALMA band-6 continuum image. The ALMA image is ≈40× deeper than the SMA image, even after accounting for the 2.6× drop in observed dust emission between 345 and 251 GHz. In all important respects the ALMA band-6 image has the same morphological characteristics as our band-7 imaging (see Fig. 2), which is more than 50× deeper than the SMA image, with a smaller and more symmetric synthesized beam. On the scales probed here, roughly 200 mas in the image plane, the dust continuum emission from the Cosmic Eyelash is remarkably smooth, not clumpy.

Spatially resolved analysis performed at the positions of the clumps identified by Swinbank et al. (2010), which we have shown here to be spurious, e.g. the work presented by Swinbank et al. (2011), Danielson et al. (2011, 2013), and Thomson et al. (2015), must be viewed in this context. The clumpy structure presented by Swinbank et al. (2010) is believed to have been generated by applying the CLEAN algorithm to noisy long-baseline SMA data, amplifying features with low signal-to-noise ratios (SNRs), where

[3]The SMA 345-GHz (rest-frame 260 μm) image of Swinbank et al. (2010) had an r.m.s. noise level of 2.1 mJy beam^{-1} (0.33×0.21 arcsec^2, PA = 15°).

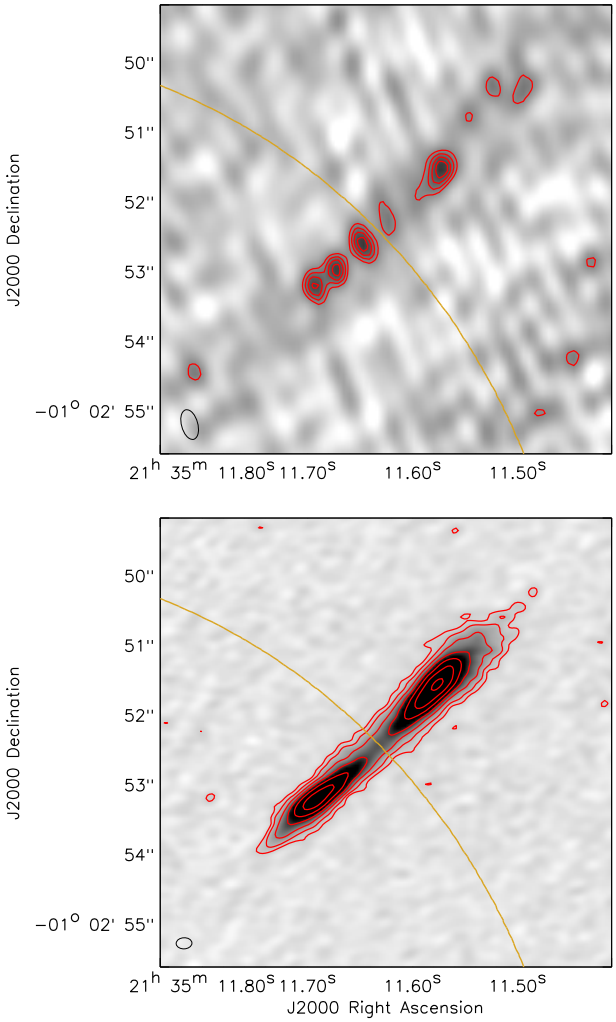

Figure 1. Top: VEX-only SMA image of the Cosmic Eyelash from Swinbank et al. (2010), where we have reproduced the contours shown in that paper as faithfully as possible, at 3, 4, 5, ..., σ, where the r.m.s., σ = 2.1 mJy beam^{-1}. Below: our observed ALMA 251-GHz (band-6) continuum image (see Section 3), which goes ≈40× deeper than the SMA image after accounting for the shape of the SED, with contours at 3, 6, 12, 24, ..., σ. Each panel has the caustic illustrated, and the respective synthesized beam.

the remarkable symmetry of the resulting structure about the likely caustic lent credibility to a clumpy morphology that we show here to be spurious. Similarities between the molecular gas morphology presented by Swinbank et al. (2011) and the spurious continuum clumps were the result of low SNR, as illustrated by the simulations of Hodge et al. (2016), which showed that high-resolution low-SNR interferometric observations yield a clumpy distribution when there are no clumps. Faced with such data, the lesson here is that an analysis like that of Hodge et al. should always be undertaken, to gauge the reality of the clumps.

4 LENS MODELLING

We have produced an updated version of the parametric mass model of the MACS J2135−01 cluster core described in Swinbank

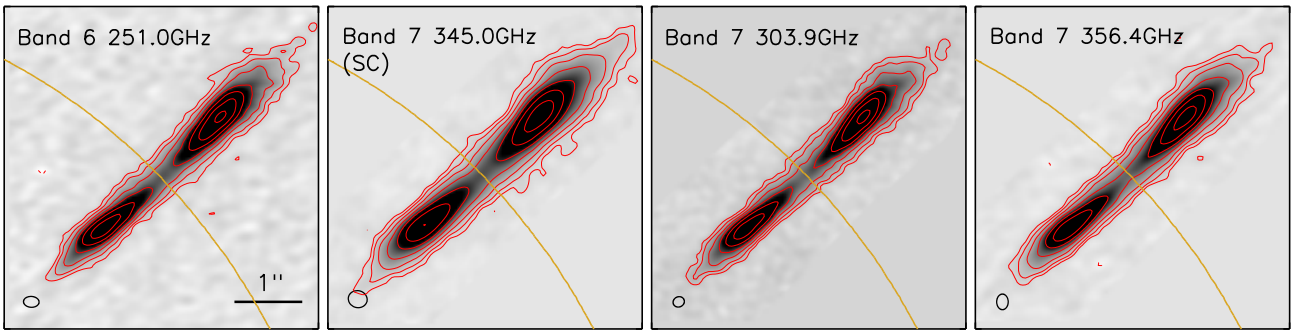

Figure 2. ALMA images of the Cosmic Eyelash, as listed in Table 1 and described in Section 3, displayed using linear greyscales from zero to the peak observed flux density, with contours at −12, −6, −3, 3, 6, 12, ..., σ. Each panel has the caustic illustrated, and also the synthesized beam, lower left.

Table 2. Best-fitting parameters for the source model to the band-7 303.9-GHz image, with extended/compact components listed top/bottom, respectively.

R_e (kpc)	Axis ratio	PA (deg)	Total flux (mJy)	Sérsic$_n$
4.42 ± 1.21	0.46	134 ± 4	6.2 ± 0.9	0.45 ± 0.22
1.23 ± 0.02	0.44	155 ± 6	8.3 ± 1.3	0.51 ± 0.06

et al. (2010) using LENSTOOL[4] (Jullo & Kneib 2009). We take the centroids of the ALMA image pair in Figs 1 and 2 as constraints.

We have used this lensing model to derive a parametric model of the source morphology at the origin of the continuum emission. We took a forward-model approach, assuming a Sérsic profile for the source, convolving by the ALMA beam and re-gridding to the same pixel grid in the image plane. The source parameters (centroid, PA, axial ratio, and FWHM) were optimized while keeping the mass model fixed. Because of a small mis-match in the lens model,[5] to reproduce both images simultaneously we performed the fit on each image independently, using the variations in the recovered parameters as an estimate of systematic errors due to the lens model.

The best source parameters with a single Sérsic profile reproduced the observed configurations well, with significant ($>50\sigma$) residuals near the core of each image, symmetrical about the critical line. Adopting a more complex parametrized source, as is becoming routine with high-fidelity ALMA data (e.g. Rujopakarn et al. 2019) – this time comprising two independent Sérsic profiles, as might be expected for a merger-induced dusty starburst (Engel et al. 2010) or for a star-forming disc with a central starburst – the resulting best-fitting source parameters gave two components lying very close in central position (within 0.01 arcsec or ≈80 pc in the source plane), but having large differences in Sérsic index and effective radii. The first one was rather extended ($R_e \sim 4.4$ kpc) while the second one was brighter and more compact ($R_e \sim 1.2$ kpc), with a small Sérsic index in both cases ($n \sim 0.5$, so at the low end of the range found by Hodge et al. 2016, but consistent, as are the effective radii). Table 2 shows the best-fitting parameters for each component.

Fig. 3 presents our best ALMA continuum image of the Cosmic Eyelash (band 7, 303.9 GHz) alongside the respective best-fitting source- and image-plane models, and residuals for the two-component Sérsic fit, where the observed map and the model are plotted with the same linear scaling (from zero to the peak observed flux density) as the residuals.

We found no mirrored sub-structure in the residual map and a brightest peak of 260 μJy, roughly 10σ above the noise; the deepest negative peaks reach 360 μJy which suggests – along with the lack of mirroring – that the sub-structure we see is not real. We followed the approach of Walter et al. (2016) to assess the fidelity of the residual peaks as a function of SNR, albeit needing to adopt large SNR bins, searching for both positive and negative peaks. We found no reliable candidates, even at 10σ: the fidelity of the brightest peaks was never better than 50 per cent. The residual peaks are all approximately consistent with the size of the synthesized beam, i.e. they are unresolved down to ≈80 pc in the source plane[6] along the major axis. If we scale the maximum positive residual, which is magnified by roughly 8× and 1.6× along the major and minor axes, to the well-sampled SED of the Cosmic Eyelash, we find that its rest-frame 8–1000-μm luminosity cannot exceed 24×10^9 L$_\odot$. Adopting the traditional conversion from L_{IR} to SFR (e.g. Kennicutt & Evans 2012) – noting that recent evidence for a top-heavy stellar initial mass function in starbursts (Schneider et al. 2018; Zhang et al. 2018b; Motte et al. 2018, cf. Romano et al. 2019) would reduce these SFR limits significantly – then corresponds to a *maximum* 'clump SFR' of 2.6 M$_\odot$ yr^{-1}, around 1 per cent of the total for the Cosmic Eyelash, at the low end of the range of SFRs reported for clumps in star-forming galaxies at $z \sim 1$–3 (e.g. Zanella et al. 2019) and consistent with the values reported via Hα observations of strongly lensed galaxies at $1 < z < 4$ (Livermore et al. 2012, 2015). Adopting the extreme starburst SED of Arp 220, our limit moves 1.6× higher.

5 SUMMARY

We present sensitive, high-spatial-resolution ALMA continuum imaging of the Cosmic Eyelash, at $z = 2.3$, which has been cited extensively as an example of where the ISM exhibits obvious, pronounced clumps, with spatial scales of ≈100 pc, and where these clumps are cited regularly as circumstantial evidence that the blue clumps observed in UV–optical images of many $z =$ 2–3 galaxies are important sites of ongoing star formation, with significant masses of stars and gas.

Our images reveal that the dust continuum emission from the Cosmic Eyelash is smoothly distributed and can be reproduced

[4] https://projets.lam.fr/projects/lenstool/wiki

[5] With our parametric model for the cluster- and galaxy-scale mass components, the two images are reproduced with a small (∼0.02 arcsec) offset, such that sending both images back to the source plane yields a small mis-match in position.

[6] Magnification varies spatially across the image plane, ranging from 3–13× along the major axis (mean, ∼10×), and ∼1.6× along the minor axis.

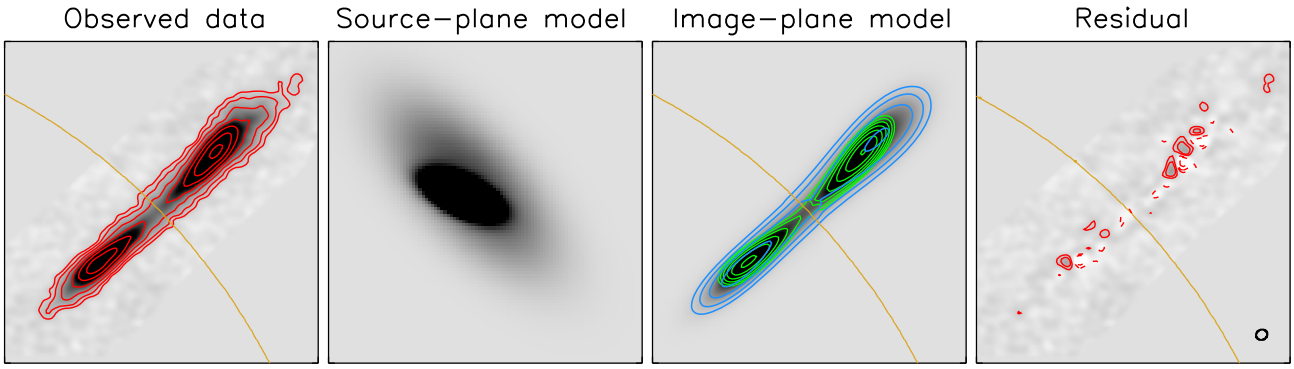

Figure 3. Left: Our most sensitive ALMA image of the Cosmic Eyelash, with the finest angular resolution, at 303.9 GHz, from the third panel of Fig. 2. Contours are plotted at −12, −6, −3, 3, 6, 12, ..., σ. Middle left and right: source- and image-plane models, respectively – see Section 4 – where the two best-fitting Sérsic profiles are contoured separately (green and blue) in the image plane, and the source-plane panel is 11.5 kpc across. Right: residuals, plotted with the same greyscale range and contours as the observed data and image-plane model. The synthesized beam is shown, lower right. Adopting the criteria of Walter et al. (2016) to assess the fidelity of the residual peaks, we find no reliable structure in the residual map.

using two coincident Sérsic profiles with effective radii, 1.2 and 4.4 kpc, with no evidence of significant star-forming clumps down to a spatial scale of ≈80 pc, with rest-frame 8–1000-μm luminosities below 24×10^9 $L_\odot$ and individual SFRs no higher than 1 per cent of the total, so $<2.6\,M_\odot\,yr^{-1}$.

ACKNOWLEDGEMENTS

Sincere thanks to the anonymous referee whose suggestions improved this paper significantly. JR acknowledges support from the ERC Starting Grant 336736-CALENDS. Funded by the Deutsche Forschungsgemeinschaft (DFG, German Research Foundation) under Germany's Excellence Strategy – EXC-2094 – 390783311.

ALMA is a partnership of ESO (representing its member states), NSF (USA) and NINS (Japan), together with NRC (Canada), MOST and ASIAA (Taiwan), and KASI (Republic of Korea), in cooperation with the Republic of Chile. The Joint ALMA Observatory is operated by ESO, AUI/NRAO and NAOJ. This paper relies on ALMA data from projects: ADS/JAO.ALMA#2012.1.00175.S, ADS/JAO.ALMA#2012.1.01029.S, ADS/JAO.ALMA#2013.1.00164.S, ADS/JAO.ALMA#2016.1.00282.S.

REFERENCES

Bisbas T. G., van Dishoeck E. F., Papadopoulos P. P., Szűcs L., Bialy S., Zhang Z.-Y., 2017, ApJ, 839, 90
Bournaud F. et al., 2014, ApJ, 780, 57
Calabrò A. et al., 2019, A&A, 632, A98
Cava A., Schaerer D., Richard J., Pérez-González P. G., Dessauges-Zavadsky M., Mayer L., Tamburello V., 2018, Nat. Astron., 2, 76
Chabrier G., 2003, PASP, 115, 763
Chevance M. et al., 2020, MNRAS, 493, 2872
Cibinel A. et al., 2017, MNRAS, 469, 4683
Conselice C. J. et al., 2004, ApJ, 600, L139
Cowie L. L., Hu E. M., Songaila A., 1995, AJ, 110, 1576
Danielson A. L. R. et al., 2011, MNRAS, 410, 1687
Danielson A. L. R. et al., 2013, MNRAS, 436, 2793
Dessauges-Zavadsky M. et al., 2019, Nat. Astron., 3, 1115
Dessauges-Zavadsky M., Adamo A., 2018, MNRAS, 479, L118
Dessauges-Zavadsky M., Schaerer D., Cava A., Mayer L., Tamburello V., 2017, ApJ, 836, L22
Dye S. et al., 2015, MNRAS, 452, 2258
Elmegreen B. G., Elmegreen D. M., 2005, ApJ, 627, 632
Elmegreen B. G., Bournaud F., Elmegreen D. M., 2008, ApJ, 688, 67
Elmegreen B. G., Elmegreen D. M., Sánchez Almeida J., Muñoz-Tuñón C., Dewberry J., Putko J., Teich Y., Popinchalk M., 2013, ApJ, 774, 86
Engel H. et al., 2010, ApJ, 724, 233
Falgarone E. et al., 2017, Nature, 548, 430
Genel S. et al., 2012, ApJ, 745, 11
Genzel R. et al., 2011, ApJ, 733, 101
George R. D. et al., 2014, MNRAS, 442, 1877
González-Nuevo J. et al., 2019, A&A, 627, A31
Gullberg B. et al., 2018, ApJ, 859, 12
Guo Y. et al., 2015, ApJ, 800, 39
Guo Y. et al., 2018, ApJ, 853, 108
Guo Y., Giavalisco M., Ferguson H. C., Cassata P., Koekemoer A. M., 2012, ApJ, 757, 120
Hezaveh Y. D. et al., 2016, ApJ, 823, 37
Hodge J. A. et al., 2016, ApJ, 833, 103
Hodge J. A. et al., 2019, ApJ, 876, 130
Ikarashi S. et al., 2015, ApJ, 810, 133
Ikarashi S. et al., 2017, ApJ, 849, L36
Indriolo N., Bergin E. A., Falgarone E., Godard B., Zwaan M. A., Neufeld D. A., Wolfire M. G., 2018, ApJ, 865, 127
Iono D. et al., 2016, ApJ, 829, L10
Ivison R. J. et al., 2010, A&A, 518, L35+
Jullo E., Kneib J.-P., 2009, MNRAS, 395, 1319
Kennicutt R. C., Evans N. J., 2012, ARA&A, 50, 531
Kruijssen J. M. D. et al., 2019, Nature, 569, 519
Larson K. L. et al., 2020, ApJ, 888, 92
Livermore R. C. et al., 2012, MNRAS, 427, 688
Livermore R. C. et al., 2015, MNRAS, 450, 1812
Ma J. et al., 2019, ApJS, 244, 30
Meng X., Gnedin O. Y., 2019, preprint (arXiv:1910.03443)
Motte F. et al., 2018, Nat. Astron., 2, 478
Oteo I. et al., 2016, ApJ, 827, 34
Oteo I. et al., 2017a, preprint (arXiv:1709.04191)
Oteo I., Zwaan M. A., Ivison R. J., Smail I., Biggs A. D., 2017b, ApJ, 837, 182
Romano D., Matteucci F., Zhang Z.-Y., Ivison R. J., Ventura P., 2019, MNRAS, 490, 2838
Rujopakarn W. et al., 2016, ApJ, 833, 12
Rujopakarn W. et al., 2019, ApJ, 882, 107
Rybak M., McKean J. P., Vegetti S., Andreani P., White S. D. M., 2015a, MNRAS, 451, L40
Rybak M., Vegetti S., McKean J. P., Andreani P., White S. D. M., 2015b, MNRAS, 453, L26
Schneider F. R. N. et al., 2018, Science, 359, 69
Simpson J. M. et al., 2015, ApJ, 799, 81
Smail I. et al., 2007, ApJ, 654, L33

Swinbank A. M. et al., 2010, Nature, 464, 733
Swinbank A. M. et al., 2011, ApJ, 742, 11
Swinbank A. M. et al., 2015, ApJ, 806, L17
Tadaki K. et al., 2018, Nature, 560, 613
Tamburello V., Rahmati A., Mayer L., Cava A., Dessauges-Zavadsky M., Schaerer D., 2017, MNRAS, 468, 4792
Thomson A. P., Ivison R. J., Owen F. N., Danielson A. L. R., Swinbank A. M., Smail I., 2015, MNRAS, 448, 1874
Walter F. et al., 2016, ApJ, 833, 67
Weiß A. et al., 2009, ApJ, 707, 1201
Wuyts S. et al., 2012, ApJ, 753, 114
Zanella A. et al., 2019, MNRAS, 489, 2792
Zhang Z.-Y. et al., 2018a, MNRAS, 481, 59
Zhang Z.-Y., Romano D., Ivison R. J., Papadopoulos P. P., Matteucci F., 2018b, Nature, 558, 260

This paper has been typeset from a TEX/LATEX file prepared by the author.